Geochemistry Geophysics Geosystems G3
AN ELECTRONIC JOURNAL OF THE EARTH SCIENCES
Published by AGU and the Geochemical Society

Article
Volume 2
December 3, 2001
Paper number 2001GC000153
ISSN: 1525-2027

Variations in slab dip along the subducting Nazca Plate, as related to stress patterns and moment release of intermediate-depth seismicity and to surface volcanism

Po-Fei Chen, Craig R. Bina, and Emile A. Okal

Department of Geological Sciences, Northwestern University, 1847 Sheridan Road, Evanston, Illinois 60208-2150, USA (bob@earth.northwestern.edu; craig@earth.northwestern.edu; emile@earth.northwestern.edu)

[1] **Abstract:** The subducting Nazca Plate shows a high degree of along-strike heterogeneity in terms of intermediate-depth seismicity (~70–300 km), orientations of slab stress, and volcanism. We compile the intermediate-depth earthquakes of South America from the Harvard Centroid Moment Tensor (CMT) catalogue to determine along-strike dip variations, and we explore the variable level of correlation between these observations. Primary results are three-fold: (1) Consistency among orientation of tension axes, highest level seismicity, and occurrence of volcanism is associated with steeply-dipping regions (20°–30°). (2) Volcanism and intermediate-depth seismicity exhibit no direct correlation, suggesting that earthquake faulting is not a necessary condition for transport of dehydrated fluids out to the mantle wedge for initiation of melting. (3) Comparison of slab thermal structures between regions with and without volcanism suggests that for certain wedge widths, the maximum temperature in the mantle wedge is higher for the former than for the latter.

Keywords: Subduction; seismicity; volcanism; stress; dip; Nazca.

Index terms: Earthquake parameters; Plate boundary-general; General or miscellaneous; South America.

Received February 23, 2001; **Revised** August 1, 2001; **Accepted** August 31, 2001; **Published** December 3, 2001.

Chen, P.-F., C. R. Bina, and E. A. Okal. Variations in slab dip along the subducting Nazca Plate, as related to stress patterns and moment release of intermediate-depth seismicity and to surface volcanism, *Geochem. Geophys. Geosyst.*, *2*, 10.1029/2001GC000153, 2001.

1. Introduction

[2] Current models for mechanisms of subduction-zone volcanism and intermediate-depth seismicity hinge on dehydration reactions of subducted hydrous minerals. For the former, it is widely accepted that evolved water reaches the hot mantle wedge to initiate melting [*Gill*, 1981; *Davies*, 1999], despite debates about actual paths of transport [*Davies and Stevenson*, 1992; *Tatsumi and Eggins*, 1995]. For the latter, a reduction in effective normal stress by liberated fluids favors brittle behavior of material in response to stresses in the slab, potentially resulting in intermediate-depth earthquakes [*Green and Houston*, 1995; *Kirby et al.*, 1996]. Consequently, the observable spatial relationships between vol-

canism and seismic features (such as hypocentral locations and stress orientations) are probably controlled by the thermal structures of slabs, which, for a given composition, govern dehydration reactions [*Schmidt and Poli*, 1998; *Ono*, 1998], fluid transport mechanisms [*Mibe et al.*, 1999] and slab stress fields [*Bina*, 1996, 1997; *Yoshioka et al.*, 1997], all functions of pressure and temperature. In this study, we investigate correlations (or their absence) in such observations along subduction zone segments of the Nazca Plate, where parameters affecting slab thermal structures (trench age, convergence rate, and dip angle) show significant variations along the trench.

[3] It has long been observed that the subducted Nazca Plate exhibits high variability in terms of volcanism, intermediate-depth seismicity, and slab shape (Figure 1). Volcanism in South America has been divided into northern (2°S–5°N), central (16°S–28°S), and southern (31°S–52°S) zones [*Thorpe et al.*, 1982], with gaps in activity between the zones. In contrast to intense intermediate-depth seismicity below the central zone, there is no seismicity below significant parts of the northern and southern zones. Under volcanic gaps, the dip angles as defined by intermediate-depth seismicity are very shallow. Thus volcanism and intermediate-depth seismicity exhibit no direct spatial relationships, while volcanism is strongly associated with more steeply dipping regions [*Cahill and Isacks*, 1992].

[4] Another property that varies with slab thermal structures, albeit in a less straightforward fashion, is the state of slab stress. In their original landmark study, *Isacks and Molnar* [1971] treated the subducting Nazca Plate as a single entity and concluded that intermediate-depth earthquakes feature overall downdip extension. This conclusion was later confirmed by considering regional variations in slab geometry [*Apperson and Frohlich*, 1987]. Given the much larger data sets of reliable seismic sources now available, we explore in the present paper variations in this general stress pattern, such as the degree of consistency of its geometric orientations, and we seek to interpret them, as well as along-strike discontinuities in volcanism, in the framework of differences in thermal regime resulting from slab geometry. We conclude that discontinuities in the Andean volcanic arc probably reflect the inability of dehydrated fluids to melt the mantle wedge overriding shallowly dipping segments of the subducting Nazca plate, owing to a field of lower temperatures in the wedge.

2. Regional Analyses

[5] Our approach is to compile the intermediate-depth earthquakes of South America from the Harvard CMT catalogue (*Dziewonski et al.* [1983] and subsequent quarterly updates) to determine the strike and dip of the subducted Nazca Plate on a regional scale. We then investigate the slab geometry in terms of its correlations with both slab stress, as revealed by CMT solutions, and volcanism, as defined by activity in the past 10,000 years [*Simkin et al.*, 1981]. Finally, in an attempt to explain the absence of volcanism in shallowly dipping regions, we examine regional differences in slab thermal structures.

[6] The spatial association between the presence of intermediate-depth seismicity, the orientations of its principal stresses, and the occurrence of volcanism must be explored in the framework of slab geometry. In order to retain some homogeneity in geometry, we partition the study area into largely latitudinal boxes in which the strike and dip of subduction are taken to be constant (Figure 1). Within each box, we define the local slab

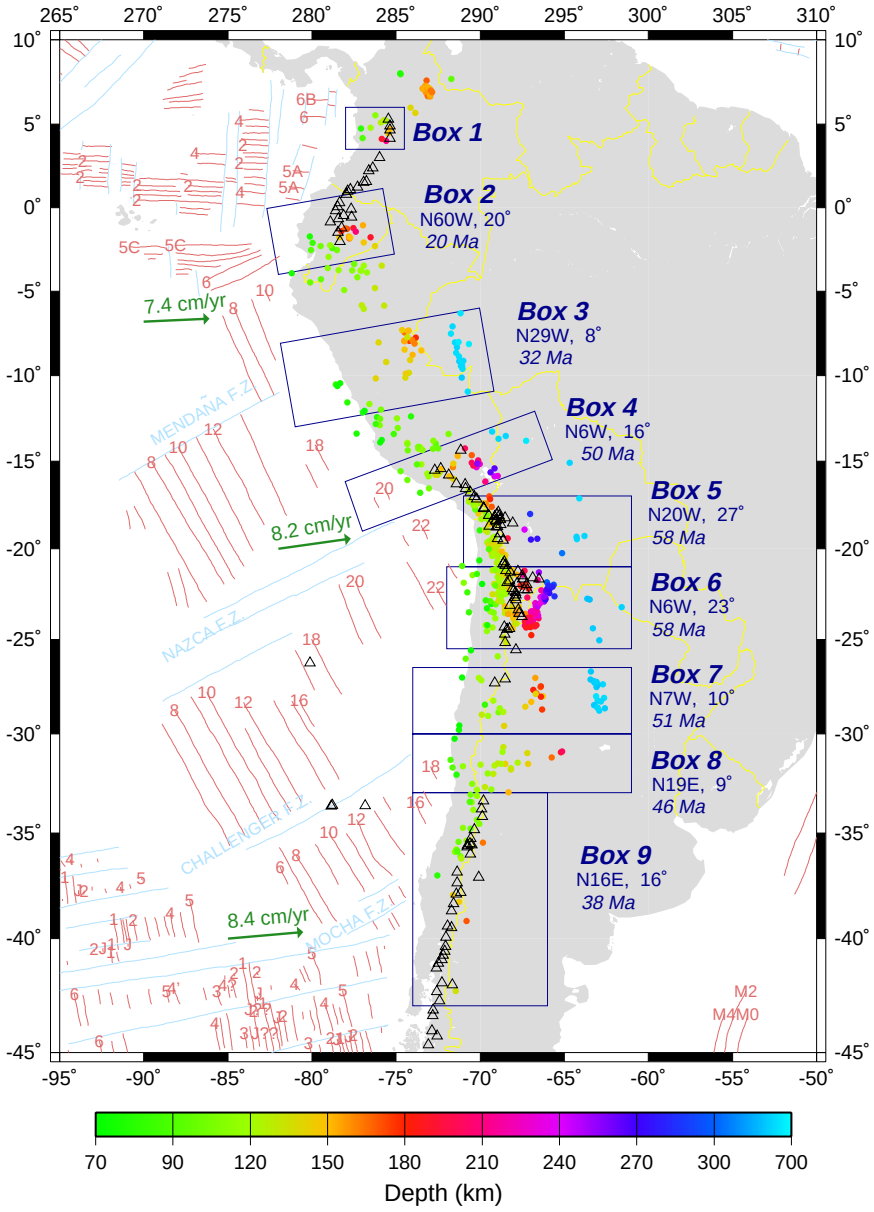

Figure 1. Partition of the study area into regional boxes. Dots, color-keyed for depth, show intermediate and deep earthquakes from the Harvard CMT catalogue. Open triangles indicate volcanoes active in the past 10,000 years. Note that both seismicity and volcanism exhibit along-strike variations. Labels for each box show slab strike and dip angles determined from this study and, in italics, the age of the oceanic lithosphere at the trench as inferred from magnetic anomalies, themselves shown as red lines on the ocean floor [*Cande et al.*, 1989]. Green arrows indicate the motion of the Nazca plate relative to South America [*DeMets et al.*, 1990].

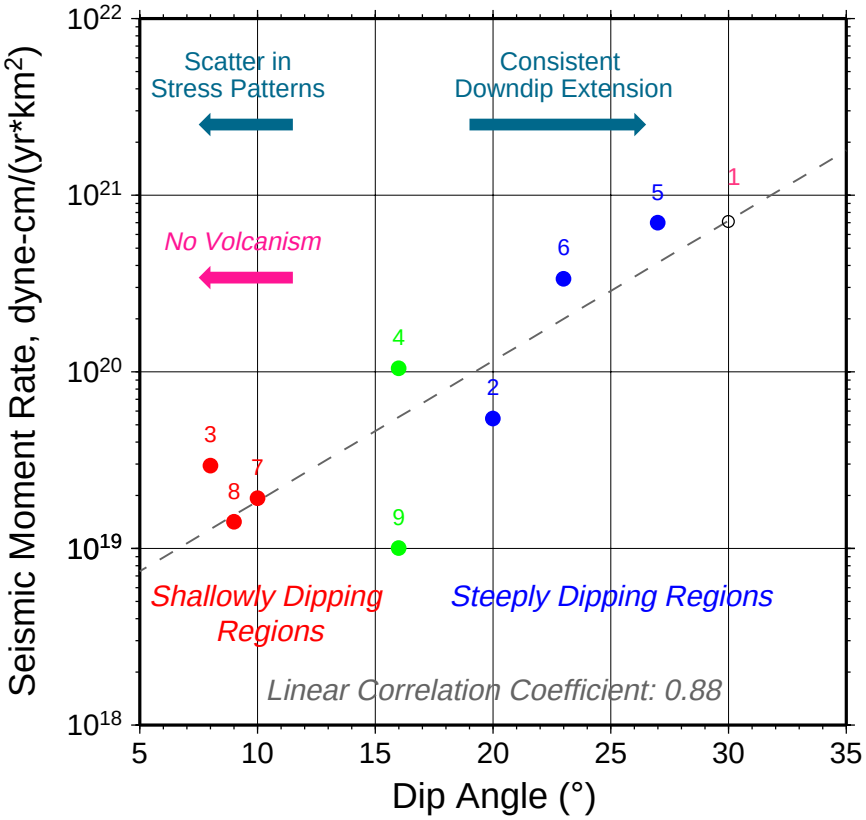

Figure 2. Seismic moment rate (normalized per unit area of subducting slab) as a function of dip angle, keyed to regional box numbers (see Figure 1). Seismic moment rate is estimated over the depth range of intermediate-depth seismicity for each box. An overall positive correlation is seen. For illustration of subsequent results, we also identify shallowly dipping regions (red group) and steeply dipping regions (blue group) and note their correlation with volcanism and stress patterns.

strike and dip angles by projecting the individual earthquake foci onto cross-section planes with different azimuths and dips and retaining the geometry of least misfit as obtained by a simple linear regression. To avoid ambiguity, the direction of strike is defined as being rotated 90° counterclockwise from the azimuth of steepest descent along the slab; this convention is consistent with the notation of the Harvard CMT solutions.

[7] Once the regional slab geometry is derived, regional volcanism is also projected onto the same plane, thereby displaying its spatial associations with the Wadati-Benioff zone. Finally, we probe the issue of regional stress patterns by projecting intermediate-depth earthquake stresses in both geographic and regional slab coordinates [*Apperson and Frohlich*, 1987].

2.1. Seismic Moment Rate Versus Dip Angles

[8] We first plot in Figure 2 the rate of moment release, obtained from the compilation of the CMT catalogue, versus dip angle, as determined by least squares in each box. The former is normalized to a unit area of

subducting slab. Note the high correlation (linear coefficient 0.88) between these two parameters, which remains robust when seismicity is binned into various depth ranges or when large events predating the digital era are included [*Chen et al.*, 2001]. We note, however, the singular behavior of region 9, which features a reduced level of seismicity. The observed dip dependence of seismic moment release suggests that an important contribution to strain energy arises from centrally directed forces, such as buoyancy, for which slab-parallel components must vary with dip angle.

2.2. Stress Patterns Versus Dip Angles and Versus Intermediate-Depth Seismicity

[9] Next we show in Figures 3–7 the geometry of stress release in each individual box using two projection systems, as illustrated in the example of box 1 in Figure 3. (Note that, eventually, we discard box 1 from the discussion on two accounts: the small number and concentrated distribution of earthquakes induce a significant variance in dip angle and the location of box 1 is near the boundary of a third plate (Caribbean Plate) whose interactions might complicate the observations.)

[10] The first projection system is geographic, derived from a north (x), east (y), down (z) Cartesian frame. We plot **P** and **T** principal stress axes using a classic lower-hemisphere equal-area projection. The second system uses the geometry of the slab, as optimized, by replacing the geographic frame with a Cartesian along-strike ("AS", ξ), slab-normal ("SN", η), downdip ("DD", ζ) system. We plot **P** and **T** axes using an equal-area projection of the positive-ζ hemisphere (Figure 3). In this fashion, the center of the projection represents the downdip direction, and the polar angle along the circle gives a measure of the angular distance from the strike of the fault in a plane perpendicular to the downdip direction.

[11] For the remaining eight boxes, we define as steeply dipping those regions with dip angles no less than 20° (boxes 2, 5, and 6) and as shallowly dipping those regions with dips no greater than 10° (box 3, 7, and 8). This difference is genuine because the magnitudes of standard deviation for dip angles are small (Figures 4, 5, 6, and 7).

[12] Overall, downdip extension prevails in the study area despite the variation in dip angles. However, upon more detailed examination, the level of consistency of this pattern is found to vary systematically with dip: while steeply dipping regions (boxes 2, 5, and 6) exhibit consistent downdip extension, shallowly dipping ones (boxes 3, 7, and 8) display a significant scatter about the mean orientation of stress. This suggests a substantial contribution of buoyancy forces to the stress field in the former (steeply dipping) regions. In the case of stress patterns and intermediate-depth seismicity, the observation that boxes 5 and 6, where stress patterns are the most consistent, also have the highest density of seismicity illustrates the importance of down-dip stresses for seismogenesis [*Bina*, 1996, 1997; *Yoshioka et al.*, 1997].

2.3. Occurrence of Volcanism Versus Intermediate-Depth Seismicity and Versus Dip Angles

[13] As mentioned above, no simple correlation can be drawn between volcanism and intermediate-depth seismicity. Although *Davies* [1999] proposed that faulting during intermediate-depth earthquakes facilitates the transport of water into the mantle wedge, thereby generating subduction-zone volcanism, the fact that the northern and southern volcanic zones overlay aseismic slab segments (between boxes

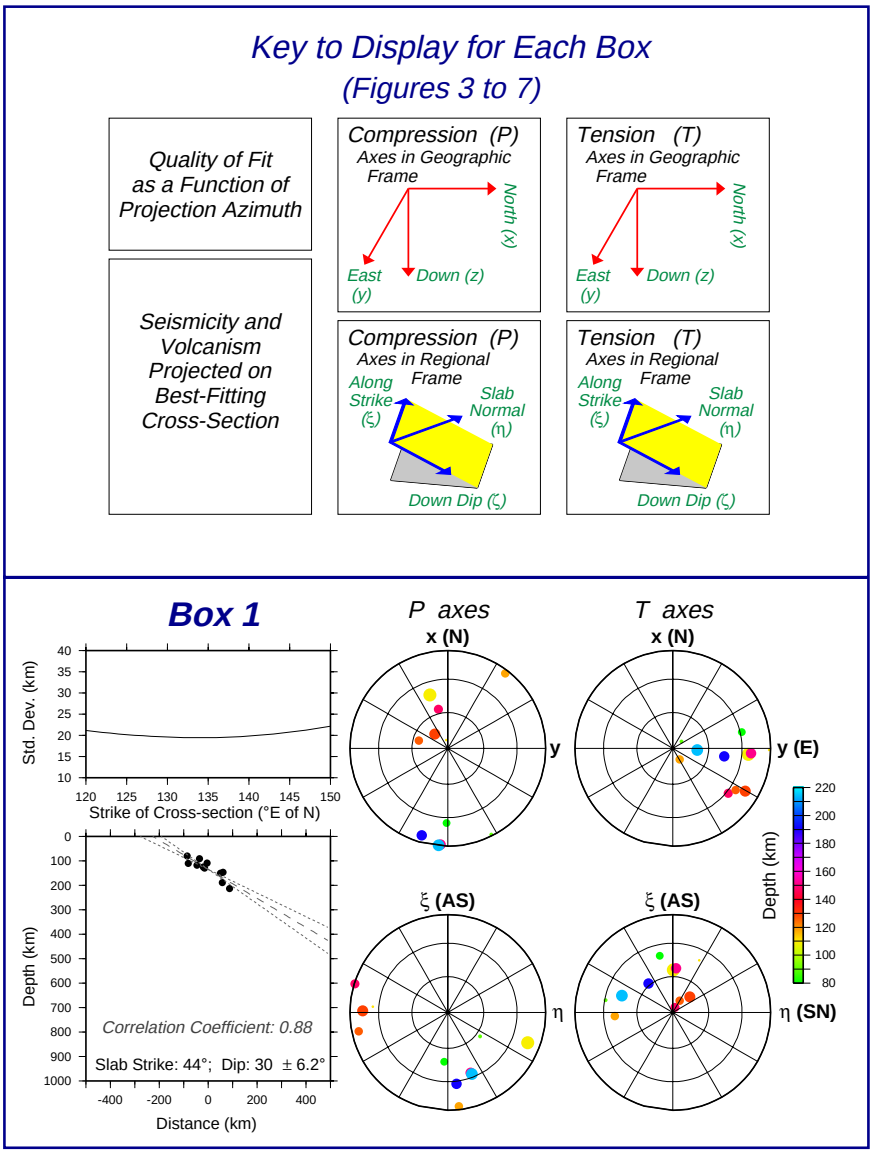

Figure 3. (top) Key to common format for display of seismicity and stress axes in each of the nine regions for Figures 3, 4, 5, 6, and 7. (bottom) Distribution of seismicity and stress release in region 1. In the upper left portion of the bottom box, quality of fit of the cross section as a function of the strike of the downdip direction on the slab is shown. The minimum of the standard deviation is used to define the strike of the best-fitting plane (rotated 90° counterclockwise from the direction of down dip). In the bottom left portion of the bottom box, the cross section of seismicity for the best-fitting geometry is shown. The dashed line is the inferred dip of the slab; the two dotted lines delimit the 1-σ errors. The top circular diagrams show **P** and **T** axes of individual CMT solutions, represented in lower hemisphere equal-area projection using the geographic frame. The bottom circular diagrams show **P** and **T** axes in regional frame. The orientation of the regional frame is explained in the key, where the slab is shown as the yellow plane and its horizontal projection in gray. Individual events are color-keyed to depth, according to the scale bar at right, with the size of the symbol related to the published moment of the earthquake.

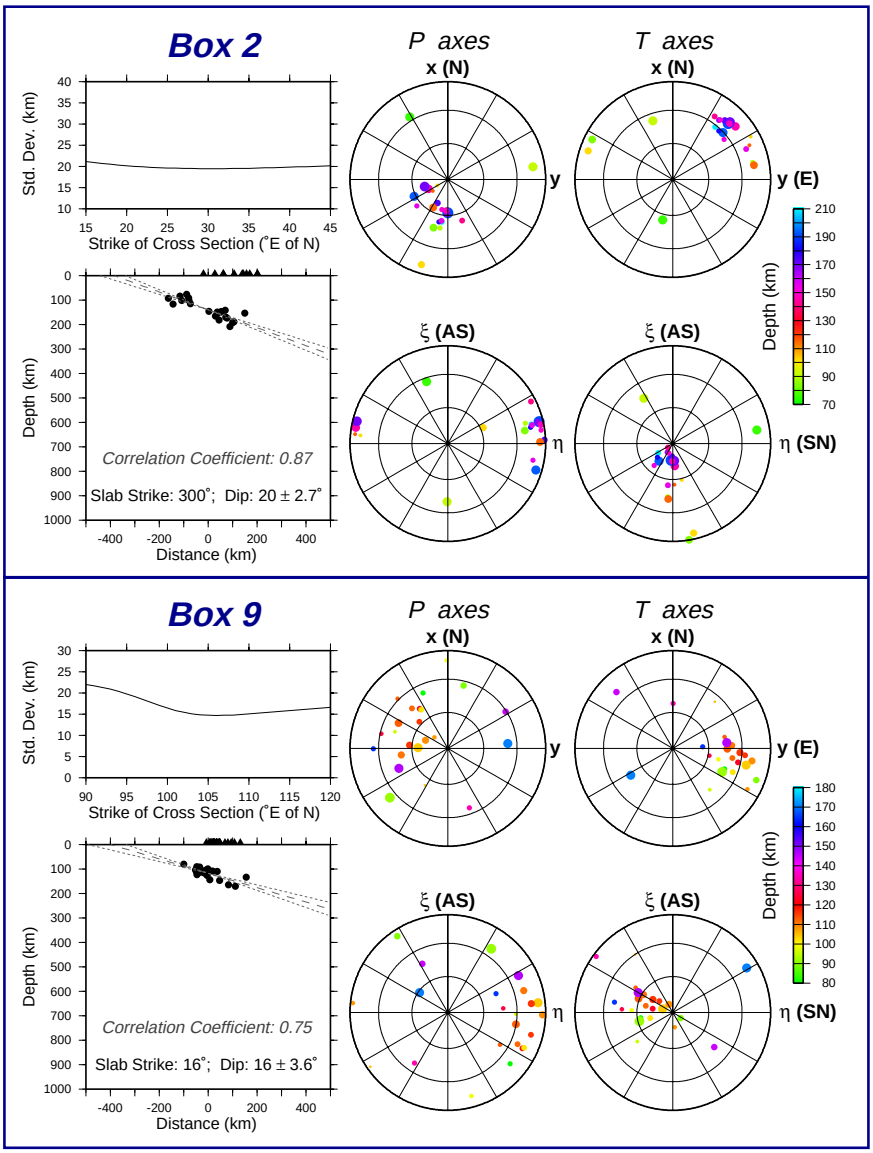

Figure 4. Results for regional boxes 2 and 9. For each box, we focus on dip angle, occurrence of volcanism, and consistency of tension axes, using the display format of Figure 3.

1 and 2, and in the southern part of box 9) suggests that this is not a necessary condition. As for correlation of volcanism with dip angles, we infer dip angles below the northern and southern zones of volcanism by extrapolating nearby intermediate-depth seismicity (boxes 2 and 9) and then investigate the correlations throughout our study area. We conclude that there is little or no volcanism at the surface above shallowly dipping regions, thus confirming the results of *Cahill and Isacks* [1992].

3. Interpretation in the Context of Volcanism

[14] The lack of consistency in the occurrence of volcanism within the same subducting

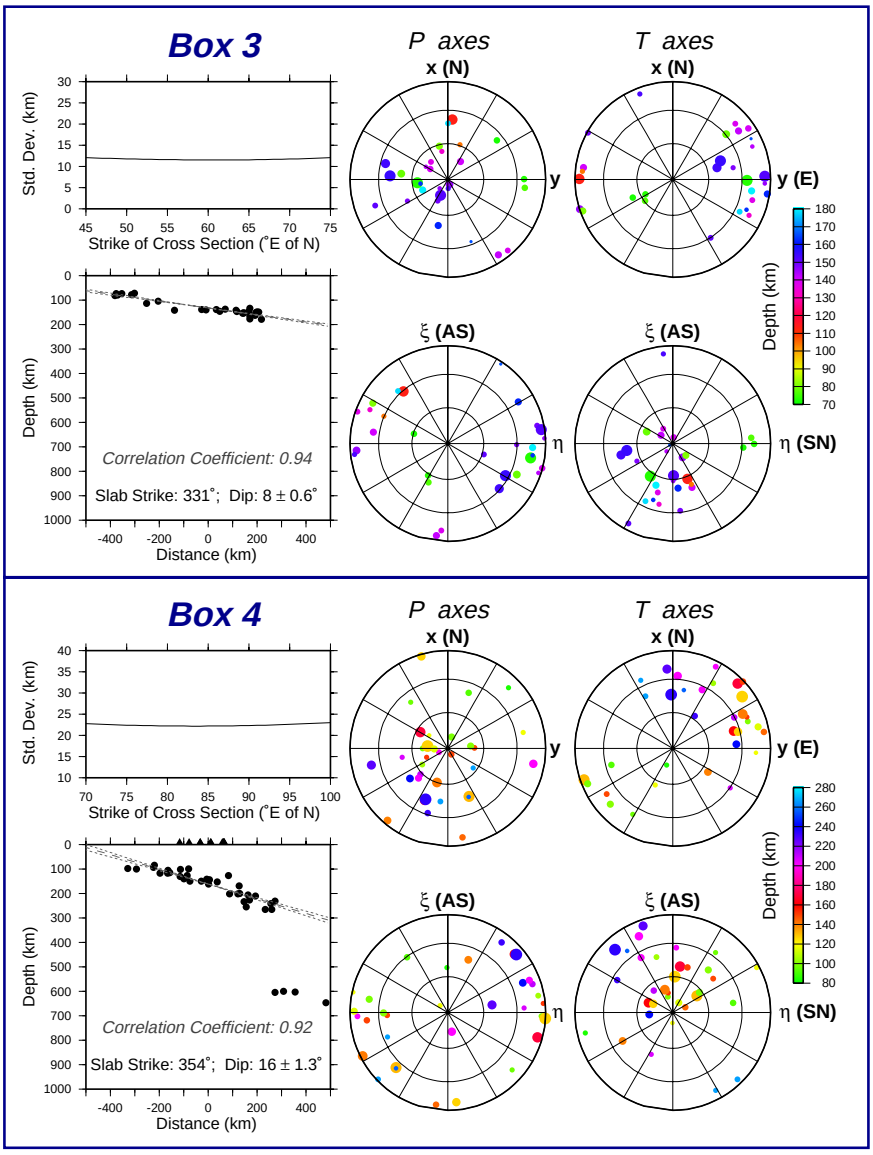

Figure 5. Same as Figure 4 for regional boxes (top) 3 (dip angle $\delta < 10°$) and (bottom) 4 ($10 < \delta < 20°$). Note the absence of volcanism in the former and its presence in the latter. Note also the scattered pattern of tension axes in both regions.

plate is particularly intriguing. In the general framework of current models for the origin of arc volcanism (as mentioned in the introduction), we propose three potential scenarios to explain the volcanic gaps observed at latitudes 3°–15°S and 28°–33°S. (1) The angle of subduction is nearly horizontal, so that almost no wedge of mantle peridotite exists, meaning that there is no material to be melted. (2) *P-T* paths along the surface of

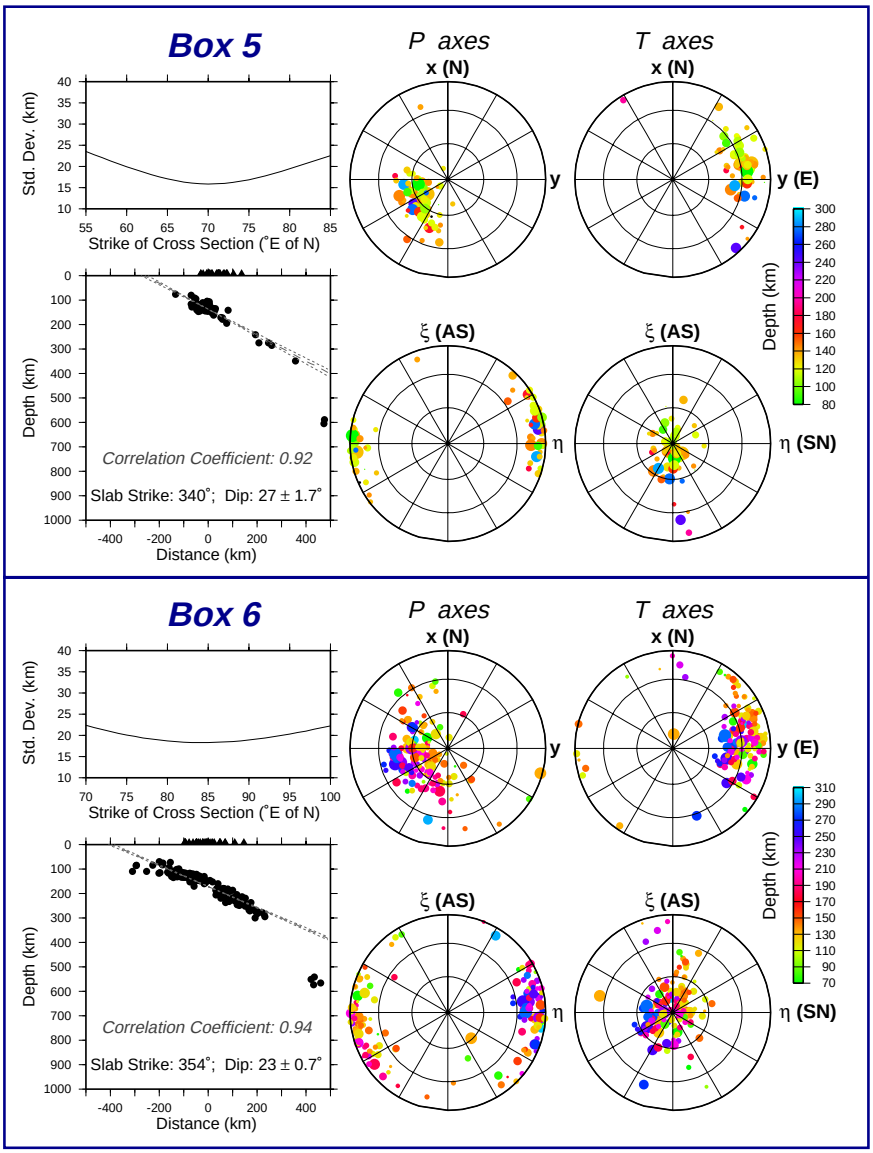

Figure 6. Same as Figure 4 for regional boxes (top) 5 and (bottom) 6; both exhibit a steep dip angle ($\delta > 20^{\circ}$), volcanism, and a high consistency of the pattern of downdip **T** axes. Also note the high level of seismicity.

shallowly dipping slabs differ significantly from those in steeply dipping slabs, so that dehydration reactions for given compositions occur at different depths. The water liberated from shallowly dipping slabs may then fail to reach the portion of mantle wedge where the temperature is suitable for melt generation from wet peridotite. (3) The *P-T* paths are similar for steeply and shallowly dipping slabs, and the water is liberated at the same

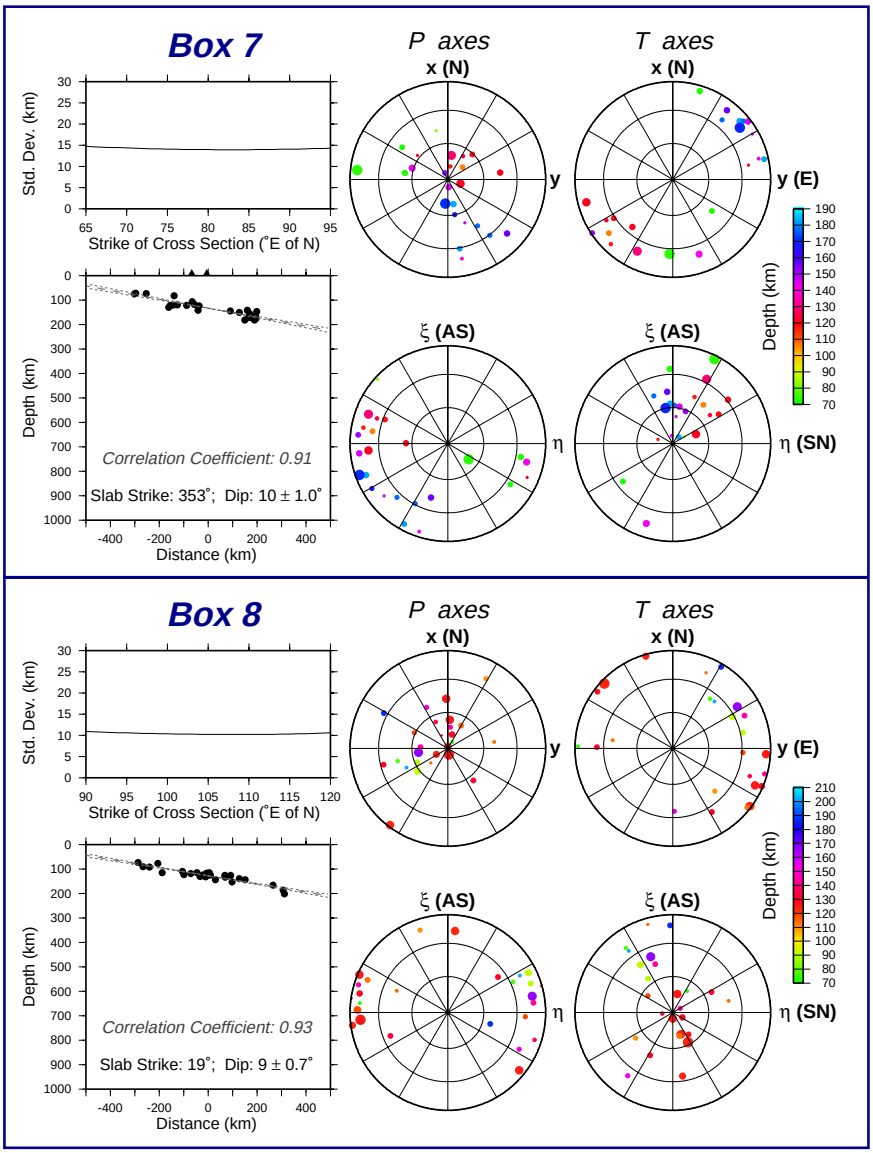

Figure 7. Same as Figure 4 for regional boxes (top) 7 and (bottom) 8; both exhibit a shallow dip ($\delta < 10^{\circ}$), no volcanism, and scattered tension axes.

depths. However, the mantle wedge just above water liberation is colder for a shallowly dipping slab than for a steeply dipping one. In this framework, there are two ways to explain the lack of volcanism in shallowly dipping slabs. The first is that the temperature in the wedge of a shallowly dipping slab is too cold to melt wet peridotite. The second is that the lower wedge temperatures induce incomplete wetting of mineral grain boundaries, by increasing the dihedral angle between forsterite (Mg_2SiO_4) grains in shallowly dip-

Table 1. Parameters Used in Thermal Modeling

Parameter	Value
Thickness of lithosphere in plate model	95 km
Density of lithosphere	3330 kg/m^3
Basal temperature of the lithosphere	1450°C
Specific heat	1.1715×10^3 J/(kg K)
Thermal conductivity	3.138 W/(m K)
Coefficient of thermal expansion (volumetric)	3.1×10^{-5} K^{-1}

ping slabs, thereby hampering development of interconnected networks for supplying aqueous fluids to the wedge [*Mibe et al.*, 1999].

[15] Scenario 1 is commonly invoked to explain such volcanic gaps [*Gutscher et al.*, 2000]. While such flat subduction may occur locally, some amount of mantle wedge material should still be present in areas of slab "sag" [*Gutscher et al.*, 2000] within these regions. Moreover, the observed persistence of seismicity to nearly 200 km depth, coupled with the presumed concentration of seismicity within the upper surfaces of slabs [*Kirby et al.*, 1996], together suggest that mantle wedge material is not wholly excluded above the subducting slab. As resolution of this issue awaits more detailed tomographic imaging, modeling of thermal structures within such wedge material is worthwhile.

[16] In order to test the feasibility of scenarios (2) and (3), we investigate the thermal structure in each individual region with the aim of resolving differences between regions with and without volcanism. We compute slab thermal structures using the finite difference algorithm of *Toksöz et al.* [1973]. For each box, the grid size is 5 km vertically, but the horizontal length varies with dip angle, in order to avoid interference with side boundaries. Given initial conditions from the GDH1 plate thermal model [*Stein and Stein*, 1992], the final temperature fields are controlled by the conduction process, the mantle geotherm being adiabatic with additional heat exchanged at phase transitions; we neglect radioactive sources and contributions from viscous dissipation [*Toksöz et al.*, 1973]. Physical parameters for all boxes are the same (Table 1). Temperature differences between individual boxes stem from variations in the following three inputs: convergence rates [*DeMets et al.*, 1990], lithospheric ages at the trenches, and dip angles. Among them, the variations in the last two are dominant for our study area.

[17] To determine the spatial relationship of seismicity and volcanism to slab thermal structures, we adopt the following reasoning: Tomographic imaging suggests that most intermediate-depth earthquakes (except in double-seismic zones) are located near the top surface of the slab [*Engdahl et al.*, 1995; *Kirby et al.*, 1996], and thermal models suggest that the coldest part of the slab lies just below the top surface at the relevant depths. Since low temperature favors brittle behavior of material, we define as the zone of seismic (or potentially seismic) activity the locus of lowest temperature in progressively deeper cross sections of the slab. Accordingly, the spatial relationship of seismicity to the slab thermal structures is determined by overlaying the line which best fits seismicity onto the line of lowest temperature within the slab (Figure 8). Finally, we project volcanism vertically down to the slab surface and plot the relevant *P-T* path for all boxes (Figure 9).

[18] Regarding the likelihood of scenario (2) above, we first note that there is no clear difference in *P-T* paths between those regions with volcanism and those without (boxes 3, 7, and 8). Furthermore, and with the possible exception of region 2, the *P-T* paths in all regions essentially sample domains of stability

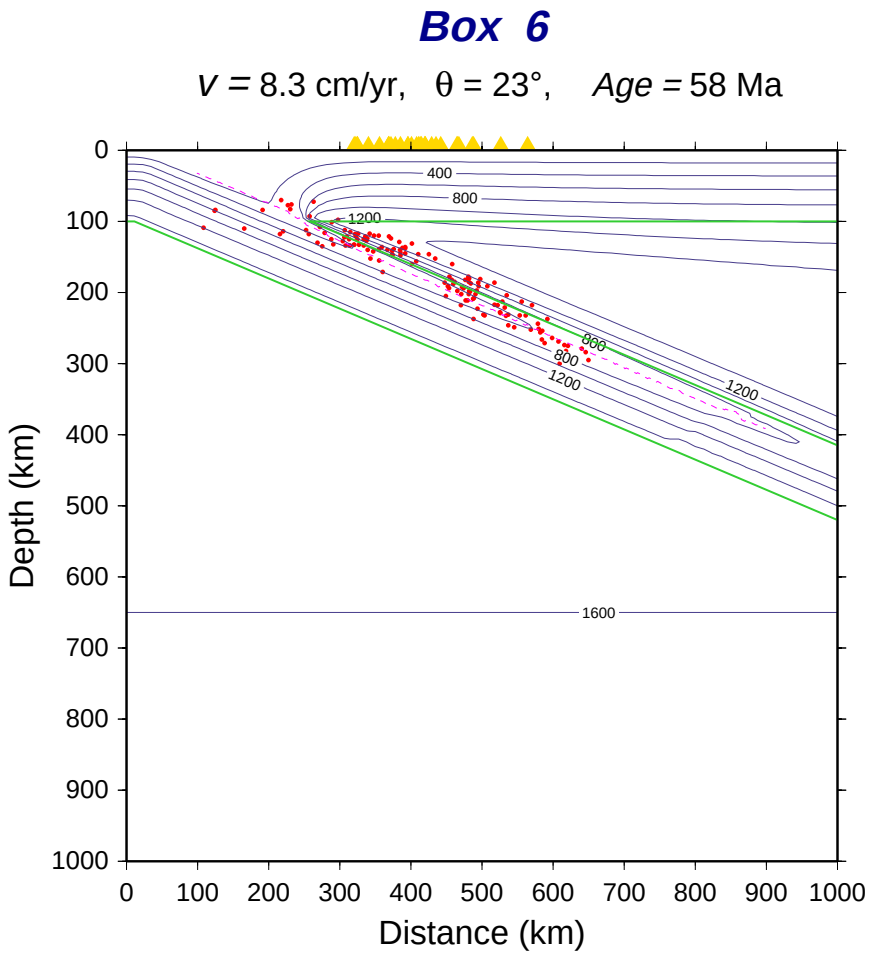

Figure 8. Portion of the thermal structure of the slab, as computed in the geometry of regional box, showing a segment extending ~1000 km in the downdip direction. Temperature contours are shown in °C. The plane of Figure 8 is the best-fitting cross section, as determined in Figure 6. The locus of minimum temperature at each depth is shown as the red dashed line, projected seismicity as red dots, and projected volcanism as yellow triangles. The inferred top surface of the subducting slab is shown as the green line and is the locus of our computation of the *P-T* path in Figure 9.

for the same assemblages. This is to say that in all regions, slab segments located under the volcanic arc (or at comparable depths in the absence thereof) undergo similar dehydration reactions. Thus we discount scenario (2) as a possible explanation.

[19] We approach scenario (3) by examining the evolution of the temperature of the mantle wedge as one moves away from the trench inside a given box. We focus on the vertical segment through the wedge that would be the potential path of buoyant H_2O liberated in the slab. The wedge thickness, H, is simply the vertical length of that segment inside the mantle, and we characterize the thermal state of the mantle wedge by the maximum temperature T_m reached along

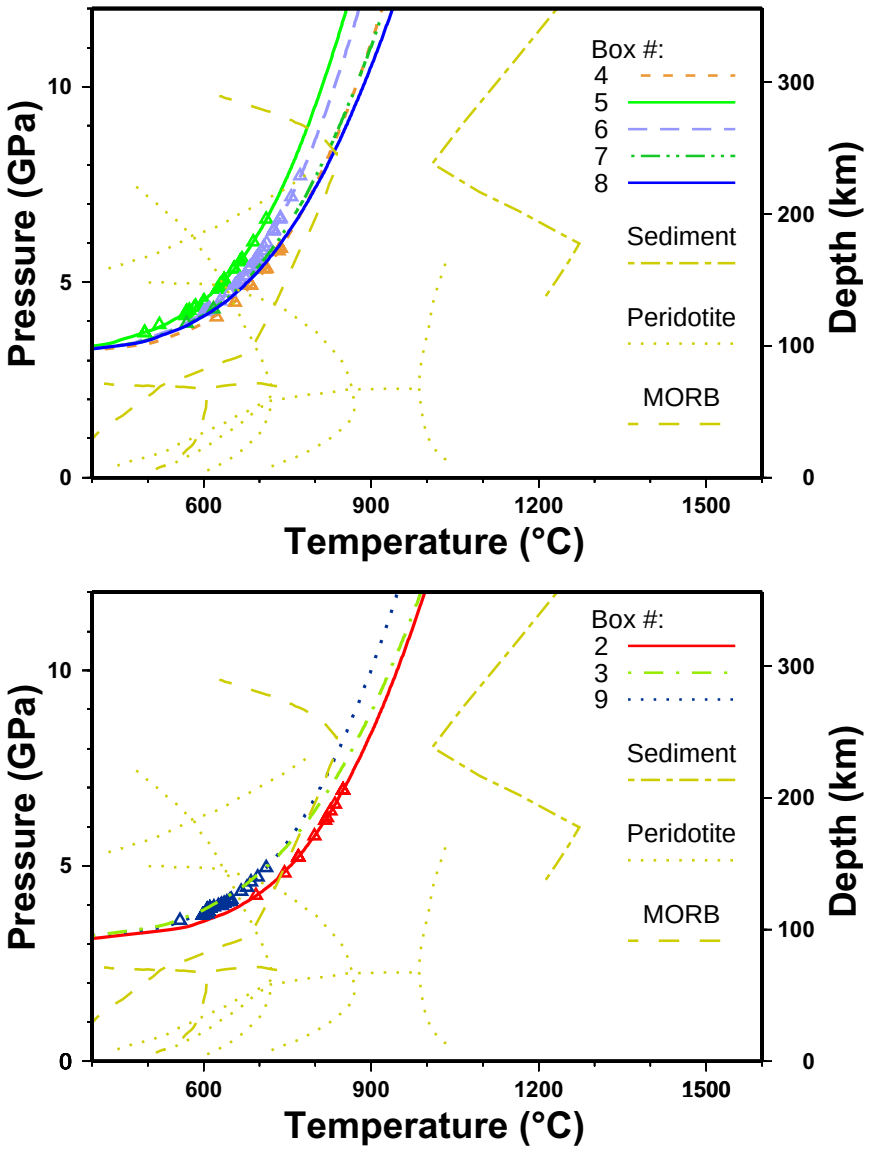

Figure 9. *P-T* paths along slab surface for different regions. (top) Regional boxes featuring older oceanic lithosphere at the trench (>45 Ma); (bottom) Regional boxes with younger lithosphere. Triangles are the relative positions of volcanic sites, vertically projected onto the surface of the slab. Dotted and dashed lines are phase diagrams of hydrous minerals present in MORB, peridotite [*Schmidt and Poli*, 1998], and sediment [*Ono*, 1998], as labeled. Note that, in both age groups, no clear distinction can be resolved in *P-T* paths for regions with and without volcanism.

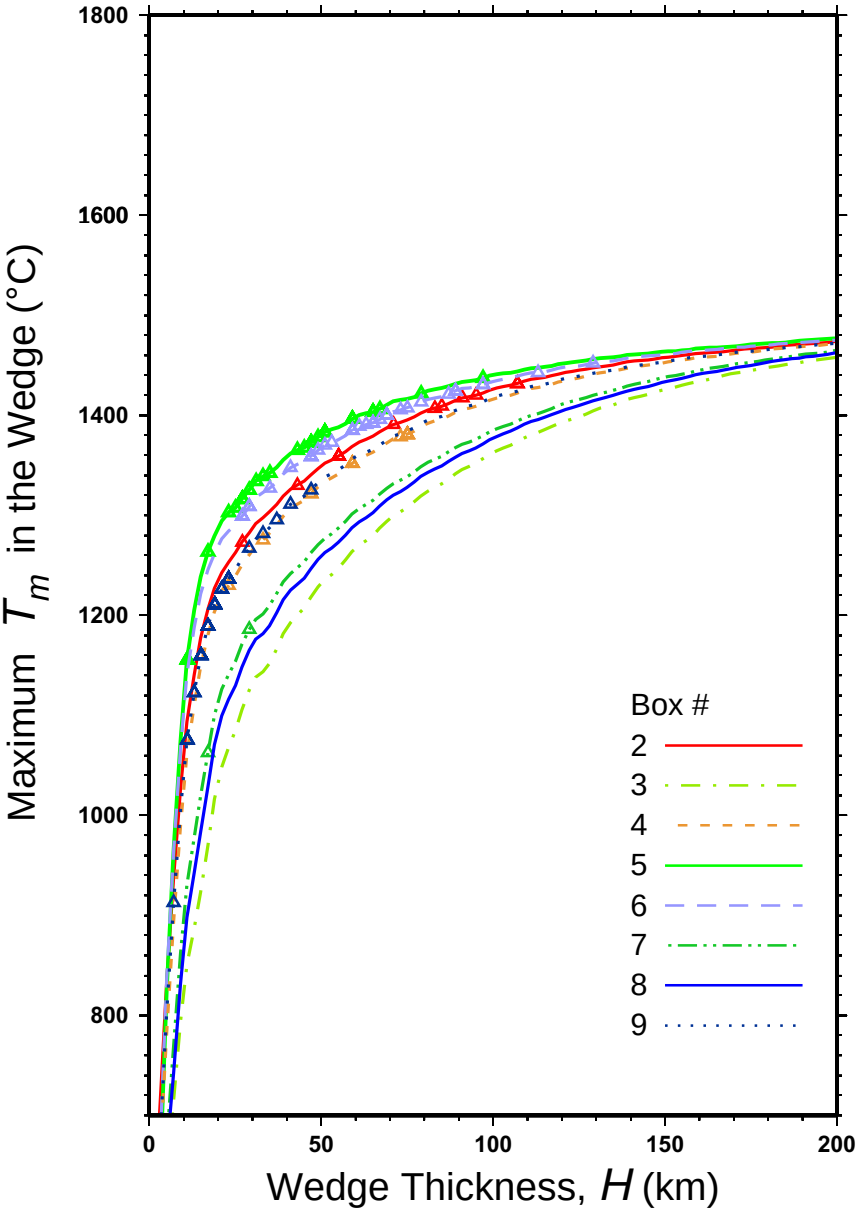

Figure 10. Maximum temperature in the overlying mantle wedge as a function of wedge width for all regional boxes. Note that the three most shallowly dipping regions (Boxes 3, 7, and 8) feature the lowest temperatures and exhibit almost no volcanism.

the vertical wedge segment. Figure 10 shows T_m *versus* H.

[20] This algorithm clearly separates regions with and without volcanism and thus favors scenario (3), in the sense that even though water is liberated at similar depths, the absence of volcanism above shallowly dipping slabs can be attributed to lower temperatures within the overlying mantle wedge. Such low temper-

atures may be below the solidus for wet peridotite, and/or may hinder fluid transport.

4. Discussion

[21] We discuss here a number of possible limitations on the methodology used for the present study. First we note that the assumption of a homogeneous slab geometry within each box might fail if the slab distorts dramatically, in which case the best planar approximation will provide only a poor fit to its geometry. Slab distortion can be decomposed into two components: trench parallel and trench normal. For the former, the use of smaller regional boxes may alleviate the extent of distortion within boxes but at the cost of reducing the number of events in each region. For the latter, we may need more parameters to describe the geometry of the slab, depending upon the extent of distortion. To see if linear fitting is appropriate, we calculate the probability that the observed data could have come from an uncorrelated parent population [*Bevington*, 1969]. It is expressed through correlation coefficients between geometrical variables (horizontal distances and vertical depths of projected seismicity). The coefficients are consistently large (average 0.90; standard deviation 0.06), and even in the worst region (box 1) the probability that the data come from an uncorrelated parent population is less than 0.001. This justifies the use of linear fitting at the intermediate-depth range.

[22] Next we address the problem of uneven seismic distributions, which might also cause errors in strike, although slab geometry is largely homogeneous in the intermediate-depth range. In such a case we would be measuring a biased apparent dip instead of the true dip. Figure 11 simulates evenly distributed seismicity on both shallowly and steeply dipping planes. Assume that strike errors are the same for both, and further project seismicity onto planes of the same azimuth relative to the true strike. We find that the standard deviation, σ, characterizing the quality of fit of the cross section is significantly less for a shallowly dipping slab than for a steeply dipping one. In other words, the misfit for a shallowly dipping slab is less sensitive to errors in strike, and thus the best-fit strike is more apt to be biased when the true seismicity is not evenly distributed or, worse, exhibits curvature. This might explain the broad minima of standard deviation versus strike in shallowly dipping regions (boxes 3, 7, and 8) and in box 4, meaning the strikes for these regions are less well constrained. Despite that, we argue that the division between shallowly dipping ($\leq 10^\circ$) and steeply dipping ($\geq 20^\circ$) slabs still holds for the following reason. In the geometry of Figure 11, the relation between true dip (θ_1), apparent dip (θ_2), and strike error (α) is given by:

$$\tan\theta_2 = \cos\alpha \times \tan\theta_1 \qquad (1)$$

Thus it would require a strike error of more than 60° to misidentify a steeply dipping slab as shallowly dipping; this is unlikely, given the generally good fit of our strikes with trench trends at the surface. Therefore our results concerning stress patterns versus dip angle remain valid despite the possible uncertainty in strikes.

[23] Finally, there remains some uncertainty, which is difficult to estimate, in the absolute slab thermal structures. However, our arguments are drawn from relative differences between slabs of various thermal structures and thus are less vulnerable to uncertainties regarding the absolute values of slab temperature. Another possible systematic error may arise from the influence of viscous coupling as an additional heat source, which we did not include in our calculations. Future work might

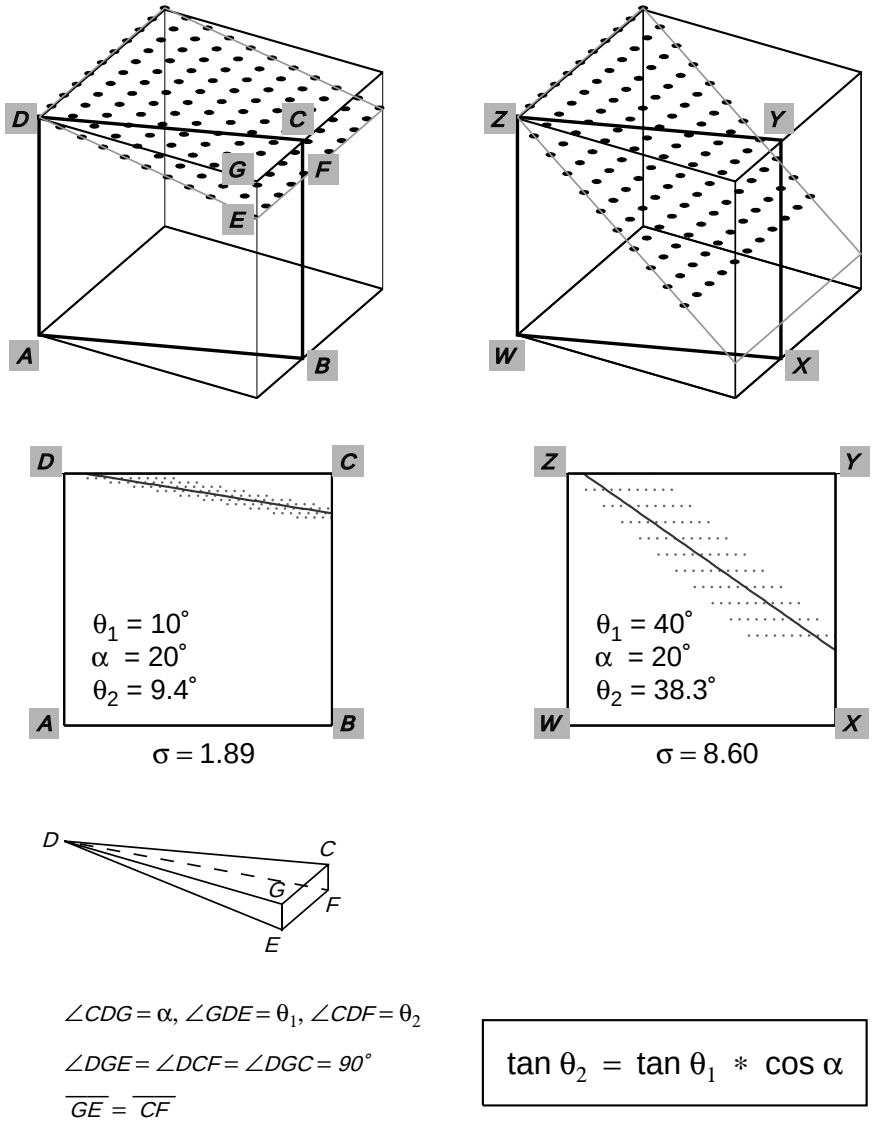

$\angle CDG = \alpha$, $\angle GDE = \theta_1$, $\angle CDF = \theta_2$

$\angle DGE = \angle DCF = \angle DGC = 90^\circ$

$\overline{GE} = \overline{CF}$

$$\tan\theta_2 = \tan\theta_1 * \cos\alpha$$

Figure 11. (top) Simulations of perfectly planar seismicity, evenly distributed on both a shallowly dipping plane (left) and a steeply dipping one (right). In both cases, seismicity is projected onto a cross-section plane (ABCD or WXYZ; shown by the thicker lines) with an azimuth error ($\alpha = 20^\circ$) with respect to the direction of true downdip. (middle) Projection of seismicity onto the best-fitting planes and corresponding best linear fits. Note that the recovered dips are slightly less than the true dips; more importantly, the shallowly dipping plane features a smaller misfit (σ) than the steeply dipping one. (bottom) Derivation of the relationship between true dip (θ_1), apparent dip (θ_2), and strike error (α).

investigate whether the trend with dip angles predicted by Figure 10 holds for thermal models incorporating viscous coupling effects.

5. Conclusions

[24] 1. Although the subducting Nazca Plate displays along-strike heterogeneity in geometry, it can still be considered locally planar in the depth range of intermediate-depth earthquakes, and the parameters of the planes can be determined by linear regression.

[25] 2. Such regressions lead to a largely bimodal distribution of slab dips, which defines shallow dips ($\leq 10^\circ$) as opposed to steep ones ($\geq 20^\circ$). We find that slab strikes are better constrained in more steeply dipping regions, and we observe that the latter also displays a higher rate of seismic moment release, as well as a more consistent orientation of tension axes in the downdip direction.

[26] 3. There is no direct correlation between volcanism and intermediate-depth seismicity, and the faulting involved in the latter is not a necessary condition for the former. However, volcanism is systematically absent from subduction segments with shallowly dipping slabs.

[27] 4. Modeling of thermal structures inside the various slab segments suggests that the lack of volcanism above shallowly dipping sections of slab may be the result of relatively low temperatures inside the associated mantle wedges, which are thus insufficient to melt or wet peridotite.

Acknowledgments

[28] We thank Ben Horner-Johnson and Fred Marton for data and codes. The paper was improved through the comments of an Associate Editor and two reviewers. Figures were generated using the Generic Mapping Tools [*Wessel and Smith*, 1995]. This research was supported by the National Science Foundation, under grant EAR-97-06152.

References

Apperson, K. D., and C. Frohlich, The relationship between Wadati-Benioff zone geometry and P, T and B axes of intermediate and deep focus earthquakes, *J. Geophys. Res.*, *92*, 13,821–13,831, 1987.

Bevington, P. R., *Data Reduction and Error Analysis for the Physical Sciences*, 336 pp., McGraw-Hill, New York, 1969.

Bina, C. R., Phase transition buoyancy contributions to stresses in subducting lithosphere, *Geophys. Res. Lett.*, *23*, 3563–3566, 1996.

Bina, C. R., Patterns of deep seismicity reflect buoyancy stresses due to phase transitions, *Geophys. Res. Lett.*, *24*, 3301–3304, 1997.

Cahill, T., and B. L. Isacks, Seismicity and shape of the subducted Nazca plate, *J. Geophys. Res.*, *97*, 17,503–17,529, 1992.

Cande, S. C., J. L. LaBrecque, R. L. Larson, W. C. Pitman III, X. Golovchenko, and W. F. Haxby, *Magnetic Lineations of the World's Ocean Basins*, scale 1:27,400,000, Am. Assoc. of Petroleum Geol. (AAPG map), Tulsa, Okla., 1989.

Chen, P.-F., M. Nettles, E. A. Okal, and G. Ekström, Centroid Moment Tensor solutions for intermediate-depth earthquakes of the WWSSN-HGLP era (1962–1975), *Phys. Earth Planet. Inter.*, *124*, 1–7, 2001.

Davies, J. H., The role of hydraulic fractures and intermediate-depth earthquakes in generating subduction-zone magmatism, *Nature*, *398*, 142–145, 1999.

Davies, J. H., and D. J. Stevenson, Physical model of the source regions of subduction zone volcanics, *J. Geophys. Res.*, *97*, 2037–2070, 1992.

DeMets, C., R. G. Gordon, D. F. Argus, and S. Stein, Current plate motions, *Geophys. J. Int.*, *101*, 425–478, 1990.

Dziewonski, A. M., A. Friedman, D. Giardini, and J. H. Woodhouse, Global seismicity of 1982: Centroid-moment tensor solutions for 308 earthquakes, *Phys. Earth Planet. Inter.*, *33*, 76–90, 1983.

Engdahl, E. R., R. D. van der Hilst, and J. Berrocal, Imaging of subducted lithosphere beneath South America, *Geophys. Res. Lett.*, *22*, 2317–2320, 1995.

Gill, J. B., *Orogenic Andesites and Plate Tectonics*, 390 pp., Springer-Verlag, New York, 1981.

Green, H. W., II, and H. Houston, The mechanics of deep earthquakes, *Ann. Rev. Earth Planet. Sci.*, *23*, 169–213, 1995.

Gutscher, M.-A., W. Spakman, H. Bijwaard, and E. R. Engdahl, Geodynamics of the flat subduction: Seismi-

city and tomographic constraints from the Andean margin, *Tectonics*, *19*, 814–833, 2000.

Isacks, B., and P. Molnar, Distribution of stresses in the descending lithosphere from a global survey of focal-mechanism solutions of mantle earthquakes, *Rev. Geophys.*, *9*, 103–174, 1971.

Kirby, S. H., E. R. Engdahl, and R. Denlinger, Intermediate-depth intraslab earthquakes and arc volcanism as physical expressions of crustal and uppermost mantle metamorphism in subducting slabs, in *Subduction: Top to bottom, Geophys. Monogr. Ser.*, vol. 96, edited by G.E. Bebout et al., pp. 195–214, AGU, Washington, D.C., 1996.

Mibe, K., T. Fujii, and A. Yasuda, Control of the location of the volcanic front in island arcs by aqueous fluid connectivity in the mantle wedge, *Nature*, *401*, 259–262, 1999.

Ono, S., Stability limits of hydrous minerals in sediment and mid-ocean ridge basalt compositions: Implications for water transport in subduction zones, *J. Geophys. Res.*, *103*, 18,253–18,267, 1998.

Schmidt, M. W., and S. Poli, Experimentally based water budgets for dehydrating slabs and consequences for arc magma generation, *Earth Planet. Sci. Lett.*, *163*, 361–379, 1998.

Simkin, T., L. Siebert, L. McClelland, D. Bridge, C. Newhall, and J. H. Latter, *Volcanoes of the World*, Smithsonian Inst., Washington, D.C., 1981.

Stein, C. A., and S. Stein, A model for the global variation in oceanic depth and heat flow with lithospheric age, *Nature*, *359*, 123–129, 1992.

Tatsumi, Y., and S. Eggins, *Subduction zone magmatism*, 211 pp., Blackwell, Malden, Mass., 1995.

Thorpe, R. S., P. W. Francis, M. Hammill, and M. C. W. Baker, The Andes,in *Andesites: Orogenic Andesites and Related Rocks*, pp. 187–205, John Wiley, New York, 1982.

Toksöz, M. N., N. H. Sleep, and A. T. Smith, Evolution of the downgoing lithosphere and mechanisms of deep focus earthquakes, *Geophys. J. R. Astron. Soc.*, *35*, 285–310, 1973.

Wessel, P., and W. H. F. Smith, New version of the Generic Mapping Tools released, *Eos Trans. AGU, Electron. Suppl.,* Aug. 15, 1995. (Available as http://www.agu.org/eos_elec95145e.html)

Yoshioka, S., R. Daessler, and D. A. Yuen, Stress fields associated with metastable phase transitions in descending slabs and deep-focus earthquakes, *Phys. Earth Planet. Inter.*, *104*, 345–361, 1997.